Analytical and numerical study of normal shock response in a uniform duct

R. V. K. Chakravarthy, Vedanth Nair, T. M. Muruganandam, and Santanu Ghosh

---

CrossMark

Analytical and numerical study of normal shock response in a uniform duct

R. V. K. Chakravarthy, Vedanth Nair,[a)] T. M. Muruganandam,[b)] and Santanu Ghosh
Department of Aerospace Engineering, Indian Institute of Technology Madras, Chennai, TN 600 036, India

The response of an inviscid shock to external pressure perturbations in a constant area duct is analyzed in terms of fundamental processes like perturbation propagation and its interaction with shock. The results of these elementary processes are formulated analytically and with a Riemann wave tracking method to enable the prediction of shock movement for both upstream and downstream perturbations. The predictions thus obtained are compared with the finite-volume based numerical simulations of the Euler equations. This study shows that the shock responds nonlinearly to perturbations and the nonlinearity has a cumulative effect. Contact surfaces generated during the interaction of normal shock with perturbations, which was ignored in previous investigations, are shown to be important in order to capture this cumulative nonlinearity. The nonlinearity alters the positive and negative duty cycles, which results in a net displacement of shock after responding to one full cycle of sinusoidal perturbation. This drift in shock location is pronounced at low supersonic Mach numbers (1.2–3) but is also present at higher Mach numbers. Furthermore, it is demonstrated that the duty cycle variations are higher for perturbations originating downstream of shock than those originating upstream. The variations in frequency and amplitude are found to merely scale the response and do not introduce any new physics. *Published by AIP Publishing.* https://doi.org/10.1063/1.5027903

I. INTRODUCTION

Steady supersonic flow with a normal shock, owing to downstream boundary conditions, is a common flow feature and occurs in supersonic intakes, nozzles, diffusers, etc. In reality, a steady flow never exists, but is often used as an idealization of the actual flow to simplify the analysis. The unsteady perturbations could be due a variety of sources, most common sources being atmospheric disturbances and those resulting from combustion process. These perturbations, in a few cases, can become very important and result in phenomena like disgorging of inlet shock, intake buzz, etc., which in turn may cause a drastic reduction in the performance of the aircraft. Hence, it is important to understand the unsteady effect due to the perturbations to gain further insight into the phenomenon plaguing the aerospace industry and take a step toward achieving better control of flight performance.

One of the earliest studies in this area is that of Hurrell.[1] He performed an analytical study of the shock response to downstream perturbations in both uniform and varying area ducts. The main focus of the study was to obtain the phase lag relation between pressure and shock movement. He showed that the shock response is instantaneous, and in the case of a constant area duct, there is no phase lag. The analysis used linearized shock relations, assumed linear wave propagation, constant shock location, and ignored the reflection of waves at the shock boundary. This work was extended by Culick and Rogers[2] to model impedance at the shock boundary and to obtain acoustic field downstream of shock. They showed that after responding to one full cycle of sinusoidal perturbation, the shock does not return to the initial position. However, they assumed the response to be a sinusoid in time to obtain this result.

Sajben *et al.*[3–5] have performed a series of experiments to study the effect of downstream perturbations in a divergent section and also to predict the frequencies at which sustained shock oscillations naturally occur. Their study focused mainly on predicting a model for impedance at normal shock boundary so that the pressure field can be calculated based on perturbations imposed downstream. As it was an experimental study, it was not possible to isolate the effect of unsteady perturbation from those due to flow separation and changes in geometry. Similar complications were faced by Bur *et al.*,[6] who have performed an experimental investigation of shock response to downstream perturbation in a divergent section. Direct Numerical Simulations (DNS) by Robinet and Casalis[7] and Oh *et al.*[8] also had the same problem.

Biedron and Adamson[9] have used asymptotic methods to obtain the shock response in a divergent duct. Their study too, like that of Culick and Rogers,[2] points toward the nonlinear response of the shock but does not give a clear reason for its occurrence. Also, as they considered a divergent section for analysis, it is not possible to conclude if the observations are due to unsteady perturbations or duct geometry.

Recent investigations include those by Moase *et al.*[10] and Bruce and Babinsky.[11] Moase *et al.*[10] have investigated the shock response in nozzles and diffusers using an analytical model to predict the shock response and impedance at the shock boundary. They further validated their analytical model by DNS of the same.

---

a)Also at Department of Aerospace Engineering, Georgia Institute of Technology, Atlanta, GA 30332, USA.
b)Author to whom correspondence should be addressed: murgi@ae.iitm.ac.in

30, 086101-1

Bruce and Babinsky[11] have performed an experimental study of the shock response in a constant area duct to downstream perturbations in a large test section area tunnel. Thus, they could avoid the complications of geometry and minimize the effect of viscosity and flow separation. However, in their investigation, when the mean shock location was oscillating, it was forced back to a desired region by manually operating the tunnel valve, and no attempt was made to investigate this phenomenon.

It can be clearly seen that most of the studies had multiple effects (flow separation, duct geometry, and unsteady perturbations) acting together. In such a scenario, it is very difficult to decouple them and attribute the observations to a single effect. Another important observation is that most of studies have tried to model the shock boundary by computing reflection and transmission coefficients at the shock boundary rather than understanding the physics of the interaction. Though the fundamental physics behind various processes involved (shock-shock interaction, nonlinear propagation of a wave) are well known, not much attention was given toward understanding the shock response from these fundamental processes.

The current study, to the best of our knowledge, is the first study which concentrates only on the effect of unsteadiness and details of the shock-perturbation interaction. This work initially analyzes a single perturbation interacting with a normal shock in a one-dimensional flow. Subsequently, a sequence of compression and expansion waves of very small magnitudes are made to interact with the normal shock. Fully analytical solution, wave tracking based semi-analytical solution, and CFD simulations are used to solve the problem and the results are compared.

A broad outline of the paper is as follows. Section II formulates the problem tackled by this study and the methodology employed. The fundamental processes mentioned in Sec. II will be discussed in detail in Sec. III. The discussion will be extended to a sinusoidal perturbation in Sec. IV to obtain an analytical formulation and various features of shock motion as predicted by this formulation will be presented. These predictions are compared against semi-analytical simulations in Sec. V and CFD simulations in Sec. VI with discussion of the results presented toward the end of each section. The conclusions are presented in Sec. VII.

II. FORMULATION AND METHODOLOGY

A. Formulation

The response of shock to a sinusoidal perturbation in pressure imposed at the boundary (both upstream and downstream) is studied with air as the fluid. The perturbation originating upstream of the shock is referred to as *upstream perturbation* and that originating downstream of the shock is referred to as *downstream perturbation*. The shock is assumed to be stationary before interacting with the perturbation and the fluid to be inviscid, non-conducting, perfect gas, and flowing through a constant area duct which is long enough such that the shock always stays inside the duct during the interaction with perturbation. If the imposed perturbation is imposed as a sinusoid at the end of the duct, it will not be a sinusoid by the time it reaches the shock and thus introduces the distance of the boundary

from the shock location as an additional parameter. To avoid this, the perturbation is assumed to attain a sinusoid profile when it just reaches the shock, i.e., the perturbation profile is not a sinusoid in space when it is generated at the boundary, but it evolves into a sinusoidal profile as it propagates from the boundary to the shock location. Under this formulation, the variation of shock response to various parameters is studied.

B. Methodology

For the interaction of a shock with a general perturbation profile, an explicit analytical solution of shock movement is not known yet.[12] As such, the analytical part of this study aims to obtain the dependence of shock response on various parameters and thus predict the qualitative characteristics of shock movement due to a sinusoidal perturbation rather than obtaining an explicit equation describing shock movement in terms of the initial perturbation profile. This prediction is then compared against a wave tracking Riemann simulation and a CFD simulation. A sinusoidal perturbation comprises of infinite number of compression and expansion waves. However, for the purpose of computation only, a finite number of waves are considered. These waves have a finite jump in flow parameters (pressure, velocity, and temperature) across them and are modeled as moving shocks. To ensure that the perturbation properties modeled through a series of shocks are same as those obtained from isentropic relations, the value of temperature corresponding to the peak value of the pressure perturbation is computed by both these methods. It is observed that the difference in the values of temperature is observed to be less than 0.01% even when a 10% variation in pressure is modeled by a single shock and this difference further reduces with number of waves. In the Riemann wave tracking method, we model the perturbations as depicted in Fig. 1(a) as a set of weak shocks (compression and expansion) approaching the stationary shock as depicted in Fig. 1(b) (note that a downstream perturbation case has been depicted in the illustration, but the same concept holds good for upstream perturbation also). Furthermore, in this study, these weak shocks are referred to as "waves" to avoid the possibility of misinterpreting the same as the stationary shock. The phase of each wave will be represented by its initial phase, ϕ_o, by the relation $\phi = kx + \phi_o$. Note that, though expansion shocks are considered, a large number of waves are considered so that the negative entropy change due to expansions is reduced and the second law of thermodynamics is not violated grossly. Furthermore, the simulations were repeated with a higher number of waves and the results did not change. In Fig. 1, ω represents the frequency of perturbation (in Hz), k is the wavenumber, P is the static pressure, P' is the amplitude of static pressure perturbation, T the temperature, and u is the flow velocity (lab fixed coordinates). The subscript "1" denotes the region upstream of shock and "2" denotes the region downstream of shock. The same notation is followed throughout the study.

Now, the problem can be further broken down into the following set of events occurring recursively till the last wave in the perturbation reaches the shock for downstream perturbation: wave approaching the shock; interacting with the shock; and the interaction of the downstream traveling residual wave
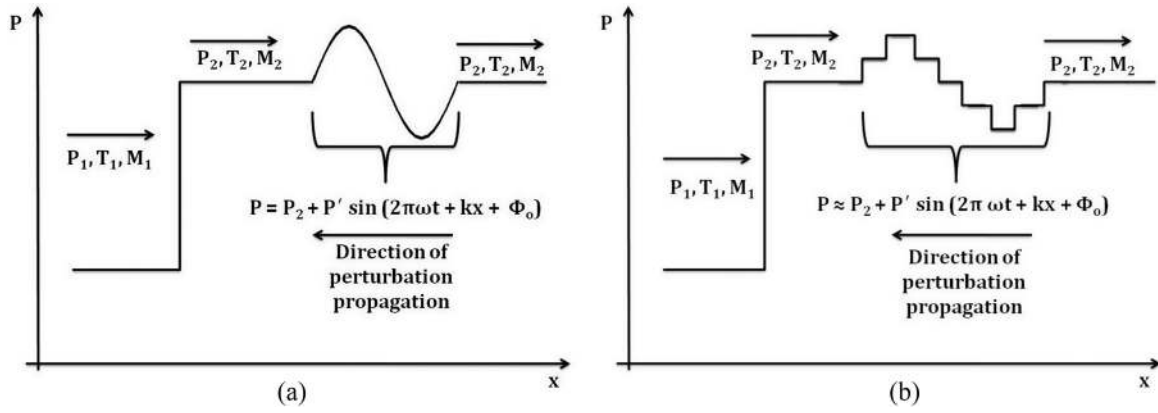
FIG. 1. Schematic representation of a shock-perturbation interaction; here the perturbation is present downstream with $\phi_o = 0$. (a) Actual flow field. (b) Approximation to the flow field.

and contact surface with upstream traveling waves. Each of these unit processes is dealt with in more detail in Sec. III. The process for upstream perturbations is the same as downstream perturbations except for the last step, which is absent, because the residual wave and contact surface generated due to shock–wave interaction exist downstream of the shock and propagate further downstream. Therefore, these cannot interact with the waves corresponding to the perturbation existing upstream of shock.

III. UNIT PROCESSES

A. Propagation of perturbation

It is well known that any perturbation profile gets distorted as it propagates. To quantify this distortion, for an initially sinusoidal perturbation, the distance (magnitude) between the peak pressure locations of linearly and nonlinearly propagated perturbations nondimensionalized by the wavelength of the perturbation is chosen as the parameter. This parameter will be referred to as the nonlinearity parameter and is denoted by ζ in further discussions. Note that by the current definition of ζ, it can vary only between 0 and 0.25. Its variation with various parameters is computed by 1-D wave tracking[13] and is presented in Fig. 2, where M_1 represents

the mean upstream Mach number, $\varepsilon = P'/P_o$, λ is the wavelength of perturbation, and subscript "o" denotes the mean value of the property of the medium into which the perturbation propagates.

It can be seen in Fig. 2(a) that the value of ζ is 0.08 at $M_1 = 2$ for a downstream perturbation of $\varepsilon = 0.04$ suggesting a significant departure from the linear propagation. Note that the legend in Fig. 2 shows a case corresponding to $\varepsilon = -0.01$ but the value of ζ is still positive because, by definition, only magnitude is considered for computing ζ. Many experimental investigations were carried out in the past in the same parameter regime ($M_1 = 1.3$–2 and $\varepsilon = 0.01$–0.04) but they were conducted in tunnels where the test section length is only about half the wavelength even for a 100 Hz perturbation. For these smaller distances, the value of ζ is close to zero[3,11] and the same result is predicted by the current study [Fig. 2(b)]. This result, ζ being close to zero, when the propagation travels a small fraction of its wavelength, has been interpreted wrongly to conclude that nonlinear propagation is negligible for any distance traveled by the perturbation. Based on this observation, many analytical studies have wrongly used linear wave propagation for their analysis.[1,2]

From Fig. 2, it is seen that the distortion for upstream perturbations is small. Apart from this, one can also see that the nonlinearity effect becomes prominent with an increase in
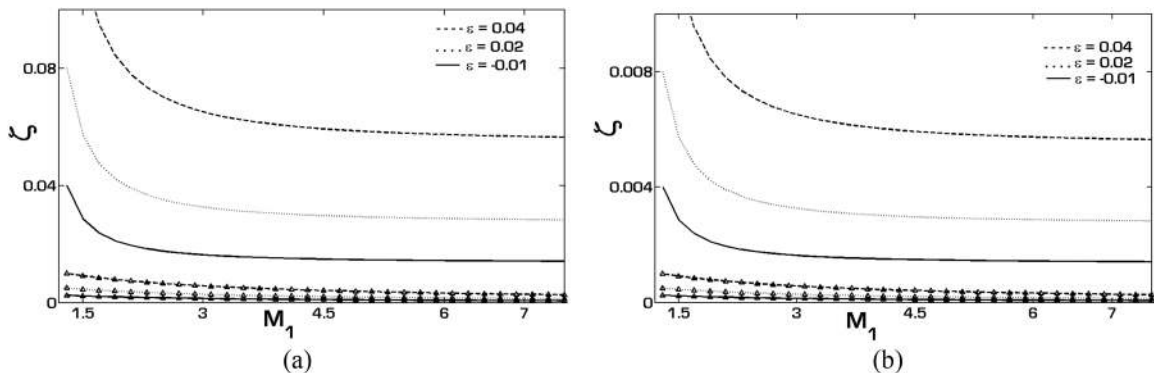
FIG. 2. Variation of nonlinearity parameter (ζ) with ε and M_1 for both upstream and downstream perturbations. The lines with "△" marker correspond to upstream perturbations and the lines with no marker correspond to downstream perturbations. The legend gives the non-dimensional perturbation jump (ε). (a) Distance travelled = λ. (b) Distance travelled = 0.1λ.

amplitude (ε) and distance traveled. It can thus be concluded that nonlinear propagation is a pronounced phenomenon and is therefore considered in this analysis.

B. Shock-perturbation interaction

As any perturbation needs to be modeled as a finite number of shocks with a small but finite jump across them (Sec. II B), the problem of shock-perturbation interaction becomes shock-shock (or shock-wave) interaction. This interaction has been discussed in the book by Hamilton and Blackstock.[14] A better approach has been given in the book by Toro[13] where the interaction creates three waves in total. The 1-D exact wave tracking (Gudonov) method used here is along the lines of the one described in the book by Toro.[13] Due to the interaction of a perturbation wave with shock, apart from altering the shock strength, a residual wave and a contact surface are additionally generated. This is illustrated in Figs. 3(a) and 3(b). The region between resultant shock and the residual wave after interaction will be referred to as the "intermediate region" and will be denoted by the subscript "*i*" in further discussions. A contact surface with temperature discontinuity exists in this intermediate region. The flow field after interaction is to be obtained numerically. It can be shown mathematically that to change a set of flow variables (P, u, T) to another set, three discontinuities are required. In special cases, these shocks could turn out to be Mach waves and contact surfaces with zero temperature discontinuity. To perform a parametric study of shock-wave (or shock/wave) interaction, a flow field consisting of a stationary shock and a single downstream wave of strength $\varepsilon = (P_3 - P_2)/P_2$ is considered as shown in the schematic (Fig. 3).

Figure 4 shows the variations in pressure, velocity, and temperature due to the shock-perturbation interaction as a function of Mach number and perturbation amplitudes. From this figure, it can be seen that the temperature jump between "*i*1" and "2" is differing from that between "*i*1" and "*i*2" by the same order as the jump between "2" and "3", showing that the residual wave temperature $'T'_{i2}$ is almost the same as $'T'_3$. The residual wave causes a very small fractional change in temperature compared to the incoming perturbation, and the incoming perturbation is itself a small fraction of the mean

pressure. It is seen that the variation of temperature across the contact surface is of the same order as the change in the primary shock strength. This clearly demonstrates that the contact surface is a very important flow feature (comparable to the perturbation) and is more significant than the residual wave. However, many analytical studies have neglected this contact surface and residual wave in their analysis. Though only downstream perturbations are quantified here, the flow features can be shown to be the same for upstream perturbation also. In the case of an upstream perturbation, however, the interaction does not have any effect on the remaining waves approaching the shock unlike downstream perturbations as the residual wave and the contact surface will travel downstream of the shock. Hence, only downstream perturbations are considered for the purpose of quantifying the flow features in a detailed manner.

C. Contact surface–perturbation interaction

The interaction of two shocks discussed in Sec. III B can be considered as flow field changing from one state to another through a series of jumps (normal shock, contact surface, and residual wave). A similar situation exists for the interaction of the contact surface with shock (or wave). Hence, the same procedure used for shock–wave interaction can be used to study the contact surface–wave interaction and as expected, the interaction results in a shock, a residual wave, and a new contact surface. The contact surface travels with the local flow velocity and this will interact with the incoming upstream propagating waves (for downstream perturbations only). For a general case of contact surface interacting with another wave, apart from the pressure jump, the velocity of the wave approaching the shock is altered. To study this interaction, a flow field with a stationary normal shock and 3 downstream waves is considered. The contact surface generated due to the interaction of the first wave with shock is allowed to interact with the remaining two downstream waves and the resultant flow fields are computed. The variation of the propagation speeds of these waves due to the interaction with the contact surface is presented in Fig. 5. Note that the waves are numbered in the order in which they reach the shock, ε_k corresponds to the jump in pressure across the *k*th wave, and the subscript denotes the property corresponding to the *k*th wave. From this figure, it can be seen that
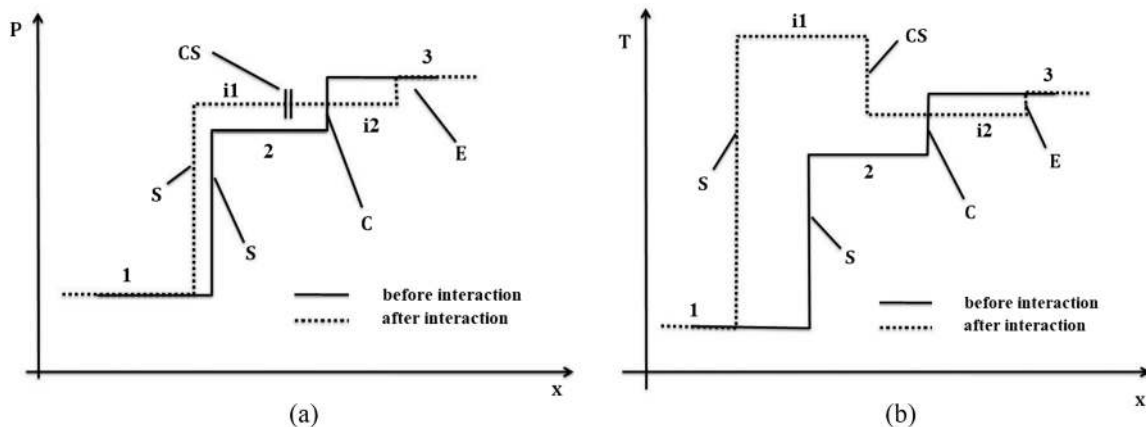

FIG. 3. Schematic representation of shock-perturbation interaction; the shock, incident compression wave, resultant expansion wave, and contact surface are represented by "S," "C," "E," and "CS," respectively. (a) Pressure. (b) Temperature.
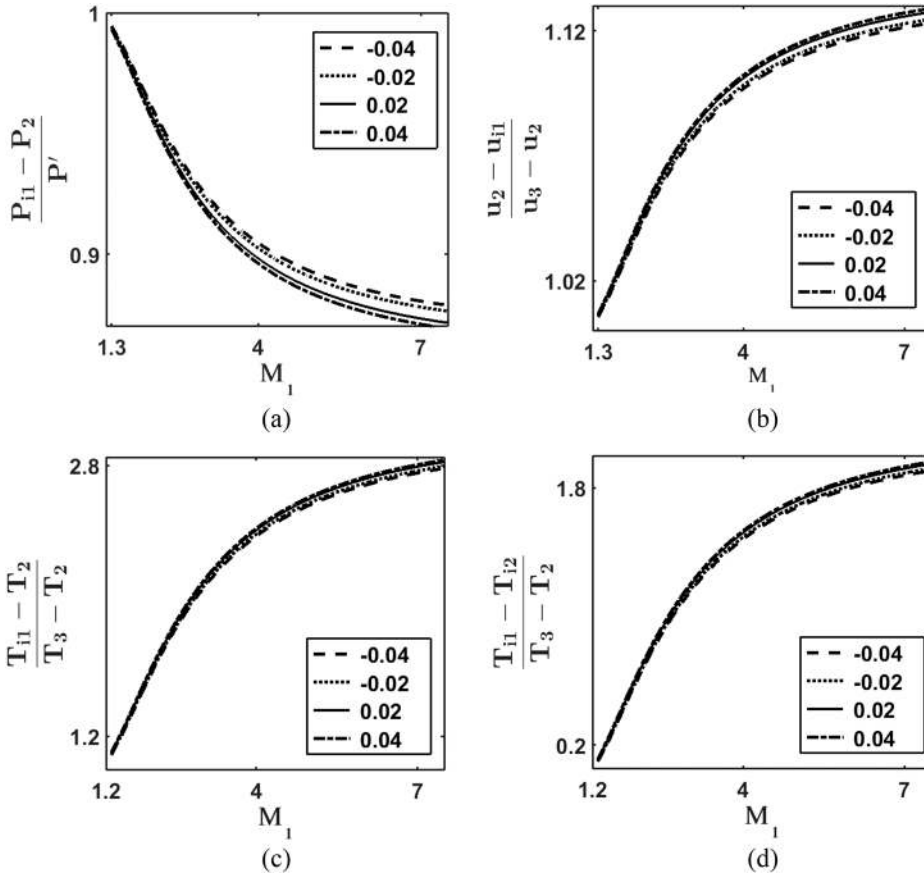
FIG. 4. Resultant flow field due to the interaction of a stationary shock with a downstream wave. The legend gives the non-dimensional perturbation jump (ε). Note that the pressure and flow velocity are continuous across the contact surface. (a) Pressure across shock. (b) Velocity across shock. (c) Temperature across shock. (d) Temperature across contact surface.

a contact surface generated due to the interaction of a shock and a compression wave increases the propagation speed of the waves on interaction and the contact surface generated due to shock interacting with expansion wave decreases the speed. Though the plots correspond to special cases of $\varepsilon_2/\varepsilon_1 = 1$ and $\varepsilon_3/\varepsilon_1 = 1$, similar trends were observed for other ratios as well. Thus, it can be concluded that the increment and decrement in speed by a contact surface is nearly the same for all the downstream waves. The change in the strength of the contact surface was found to be negligible due to interaction with the upstream traveling perturbation waves.

IV. ANALYTICAL STUDY

A. Formulation

Consider a sinusoidal perturbation approaching the stationary shock discretized into a finite number of waves/shocks as shown in Fig. 1(b). It is seen in Sec. III that each wave propagates at a different speed, alters the relative velocity of the next wave in the shock fixed coordinate system, and the relative velocity is further altered by the contact surface. These velocity changes are just dependent on jump in pressure across the waves and independent of the distance between

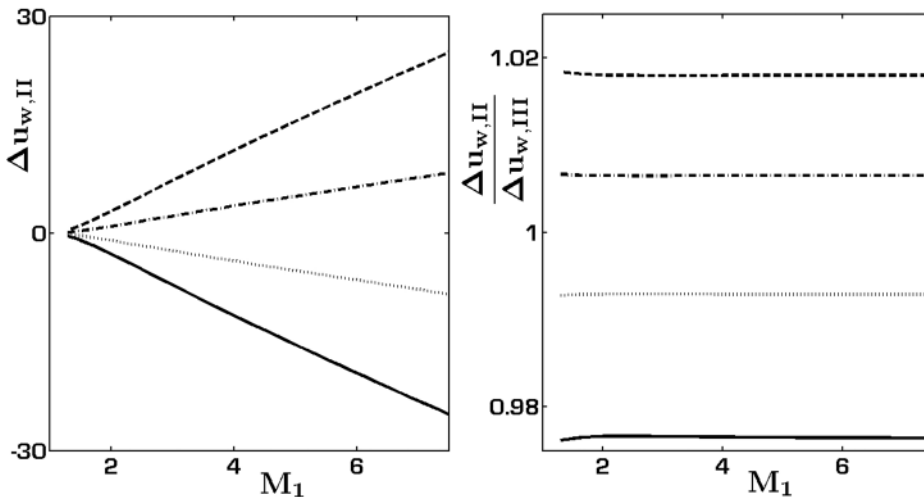FIG. 5. Variation of various velocities due to interaction of a contact surface with a downstream wave for $\varepsilon_2/\varepsilon_1 = 1$ and $\varepsilon_3/\varepsilon_1 = 1$. Each line represents a value of ε_1. Solid line (—): −0.06, dotted line (· · ·): −0.02, dashed-dotted line (−·−·−): 0.02, and dashed line (- - -): 0.06. The downstream waves are numbered in the order they reach the shock.

them. However, these changes in velocity alter the relative distance between waves and accumulate with time. Of the three phenomena mentioned, nonlinear propagation, shock movement, and contact surface interactions, only shock movement does not alter the distance between waves and is therefore only a local nonlinearity, whereas other two effects are cumulative nonlinearities. Please note that as the effect of the residual wave is small, it is neglected for the analysis. Also note that though the schematic (Fig. 1) depicts a special case of downstream perturbation, the analysis presented next will hold good for any upstream and downstream perturbations.

Let the perturbation be discretized into n waves with the first wave reaching the shock at time $t = 0$, labeled as "1," and the velocity at which each wave approaches the shock be denoted by u. Note that all the velocities are stated in a ground fixed coordinate system. Let the time at which the ith wave reaches the shock be denoted by $t(\phi_i)$, $\Delta t(\phi_i)$ be the additional time required by the ith wave to reach the shock after the $(i - 1)$th wave reached the shock, and $\Delta x(\phi_i)$ be the relative position of the $(i - 1)$th wave with respect to the ith wave at time $t(\phi_i)$. Let the velocity of shock after interaction with the ith wave be $u_s(\phi_i)$. Assume the discretization of the sinusoidal perturbation to be such that the waves are uniformly spaced at time $t = 0$ with the spacing denoted by Δx_o [i.e., relative position of the $(i - 1)$th wave with respect to the ith wave at $t = 0$] and the phase $(kx + \phi_o)$ of each wave be denoted by ϕ_i. The mean propagation velocity of all the waves in the perturbation is u_o and the propagation velocity of any individual wave is $u(\phi_i)$. Note that displacements and velocities in the upstream direction are assumed to be positive for this section only. Writing the expression for $\Delta t(\phi_i)$ in the shock fixed coordinate system, we get

$$\Delta t(\phi_i) = \frac{\Delta x(\phi_i)}{u_{avg}(\phi_i) - u_s(\phi_{i-1})} \tag{1}$$

and

$$t(\phi_i) = \sum_{j=1}^{i} \Delta t(\phi_j). \tag{2}$$

Note that in the case of upstream perturbations, the signs of both the numerator and denominator will change naturally and the formulation holds good. As the value of $\Delta x(\phi_i)$ and $u_{avg}(\phi_i)$ depend on various phenomena, to account for the contribution of each effect, they can be decomposed as

$$\Delta x(\phi_i) = \Delta x_o + \Delta x_n(\phi_{i-1}) + \Delta x_c(\phi_{i-1}), \tag{3}$$

$$u_{avg}(\phi_i) = u_o + u_n(\phi_i) + u_c(\phi_{i-1}) + \epsilon, \tag{4}$$

where $\Delta x_n(\phi_{i-1})$ is the change in the relative distance between the $(i - 1)$th and ith wave with respect to the ith wave due to nonlinearity in perturbation propagation till time $t(\phi_{i-1})$, $\Delta x_c(\phi_{i-1})$ is the change in the relative distance between the $(i - 1)$th and ith wave with respect to the ith wave due to their interaction with the last $(i - 2)$ contact surfaces, $u_n(\phi_i)$ is $(u(\phi_i) - u_o)$ at $t = 0$, $u_c(\phi_{i-1})$ is the change in the propagation velocity of the ith wave due to interaction with $(i - 2)$ contact surfaces (i.e., $u(\phi_i)|_{t=t(\phi_{i-1})} - u(\phi_i)|_{t=0}$), and ϵ is the difference in the average velocity of the ith wave due to the interaction with the $(i - 1)$th contact surface.

As ϵ represents the effect due to a single contact surface, it is negligible compared to contribution of $(i - 2)$ waves represented by $u_c(\phi_{i-1})$ and is neglected for further analysis. Substituting Eqs. (3) and (4) into Eq. (1), non-dimensionalizing lengths by Δx_o and velocities by u_o in Eq. (1), performing a binomial expansion on the denominator of the resulting expression and retaining terms till $O(\varepsilon)$, we get

$$\Delta t(\phi_i) = \Delta t_o [1 + \delta x_n(\phi_{i-1}) + \delta x_c(\phi_{i-1}) - \delta u_n(\phi_i) \\ - \delta u_c(\phi_i) + \delta u_s(\phi_{i-1})], \tag{5}$$

where $\Delta t_o = \Delta x_o / u_o$ is the $\Delta t(\phi)$ for any wave in a linearly propagating perturbation and $\delta\beta$ represents the non-dimensional version of the variable β. Of the five terms in Eq. (5), only the velocity terms are purely functions of phase and can be analyzed by considering flow fields similar to those considered in Secs. III B and III C. However, as the displacement terms are cumulative nonlinearities, such an approach is not possible, but a functional dependence of these terms on δu terms can be obtained to proceed further with the discussion.

B. Distortion due to nonlinear propagation

The total distance altered between two consecutive waves due to nonlinear propagation is

$$\delta x_n = \frac{u(\phi_{i-1}) - u(\phi_i)}{\Delta x_o}[t_{initial} + t_s], \tag{6}$$

where $t_{initial}$ is the time taken by the $(i - 1)$th wave to reach the shock position (x_s) at $t = 0$ and t_s is the additional time required to reach the shock from $x_s(t = 0)$. As mentioned earlier, δx_n is a non-dimensional variation in the distance between the $(i - 1)$th and ith wave due to the nonlinearity in their respective propagation speeds. It is to be noted that in writing the above expression, the observation that the contact surface alters the velocity of all the upstream traveling waves by nearly the same amount is utilized. Thus, the term $(u(\phi_{i-1}) - u(\phi_i))$ can be assumed constant in time. Substituting Eq. (5) in Eq. (2), we get

$$t(\phi_i) = \hat{T}(\phi_i)[1 + \delta] = i\Delta t_o(1 + \delta), \tag{7}$$

where $\hat{T}(\phi_i)$ is the time taken by the ith wave to reach $x(\phi_1)|_{t=0}$ in the case of a linearly propagating wave in the absence of shock (i.e., pseudo-shock in Sec. IV D) and δ is the resultant of $O(\varepsilon)$ terms. Substituting Eq. (7) in Eq. (6), rewriting temporal terms, and expanding all the individual terms in to $O(\varepsilon)$, we get

$$\delta x_n \approx \left[\frac{(1 + \delta u_n(\phi_{i-1})) - (1 + \delta u_n(\phi_i))}{1 + \delta u_n(\phi_{i-1})} \right](i - 1) \\ \times \left[\frac{1 + \delta u_s(1 + \delta)}{1 + \delta u'(\phi_{i-1})} \right], \tag{8}$$

where $\delta u'(\phi_{i-1})$ is a $O(\varepsilon)$ term representing the expansion of $u_{avg}(\phi_{i-1})$ about $u(\phi_{i-1})$. The derivation of this expression is given in the Appendix. Simplifying Eq. (8) using the binomial expansion to the $O(\varepsilon)$ term, we obtain

$$\delta x_n(\phi_{i-1}) \approx [\delta u_n(\phi_{i-1}) - \delta u_n(\phi_i)](i - 1) \propto max\{\delta u_n(\phi_j)\}, \\ j \in 1, 2, \dots, n. \tag{9}$$

From this expression, we see that δx_n is proportional to δu_n and is independent of the displacement of shock due to perturbation

suggesting that it is a higher order effect though the shock velocity (δu_s) is of $O(\varepsilon)$.

C. Distortion due to contact surface interaction

During the time the contact surface takes to travel between two waves, the difference between the propagation speeds results in contraction/stretching of the distance between the two waves. This effect is computed as follows:

$$\delta x_c(\phi_{i-1}) = \sum_{j=1}^{i-2} \Delta u_c(\phi_j) \Delta t(\phi_j) \frac{1}{\Delta x_o}, \qquad (10)$$

where $\delta t(\phi_j)$ is the time taken by the jth contact surface to travel from the $(i-1)$th wave to ith wave and $\Delta u_c(\phi_j)$ is the change in velocity due to the interaction with the jth contact surface. In the contact surface fixed coordinate system, the term $\Delta t(\phi_j)$ can be approximated as

$$\Delta t(\phi_j) \approx \frac{\Delta x^j(\phi_i)}{c^j(\phi_i)}, \qquad (11)$$

where $\Delta x^j(\phi_i)$ is the distance between the $(i-1)$th and ith wave after the interaction of the jth contact surface with the $(i-1)$th wave and $c^j(\phi_i)$ is the local speed of sound between these waves. Substituting this expression in Eq. (10) and retaining terms till $O(\varepsilon)$, we get

$$\delta x_c(\phi_{i-1}) \approx \sum_{j=1}^{i-2} \frac{\Delta u_c(\phi_j)}{u_o} \frac{u_o}{c_o} = (1 - M_2)\delta u_c(\phi_{i-1}). \qquad (12)$$

D. Predictions

Consider the case of a downstream sinusoidal pressure perturbation with $\phi_o = 0$ traveling in a uniform flow (i.e., shock is absent) toward a stationary surface with zero jump in flow properties across it (this surface will be referred to as "pseudo-shock" in further discussions). Applying Eq. (5) to this flow field, we get

$$\Delta t(\phi_i) = \Delta t_o[1 + \delta x_n(\phi_{i-1}) - \delta u_n(\phi_i)]. \qquad (13)$$

We know that for two consecutive compression waves, $\delta x_n < 0$, whereas $\delta x_n > 0$ for two consecutive expansion waves and $\delta u_n > 0$ for the entire positive half cycle of perturbation. However, the time at which the wave corresponding to $\phi = \pi$ reaches the pseudo-shock is $0.5\bar{T}$, where $\bar{T}$ is the time period of the perturbation. For this to be possible, the net effect of Δx_n over the positive half cycle should match that of Δu_n.

For the case of downstream perturbation with a shock, the analysis is not as straightforward as in the case of pseudo-shock as all the terms in Eq. (5) are to be considered. As there are no explicit analytical expressions for these terms, the relative quantitative effects of these terms are obtained numerically. Consider a flow field with a stationary shock and two downstream waves. The interaction of the first wave with the shock and the interaction of the resulting contact surface with the other wave is studied. Thus, the various δu terms are computed and the results are given in Fig. 6. Using Eqs. (9) and (12), the dependence of δx on M_1 and ε can be obtained.

Using these results, the resultant shock response can be predicted. In the absence of the nonlinearities discussed in Sec. III, the response is known to be a sinusoid in time. As an exact solution is not possible for the case which includes the nonlinearities; the analysis will only predict the data at 4 points ($\phi = 0.5\pi$, π, 1.5π, and 2π) and thus construct the shock response by tweaking the sinusoidal response accordingly. The response to downstream perturbations is discussed
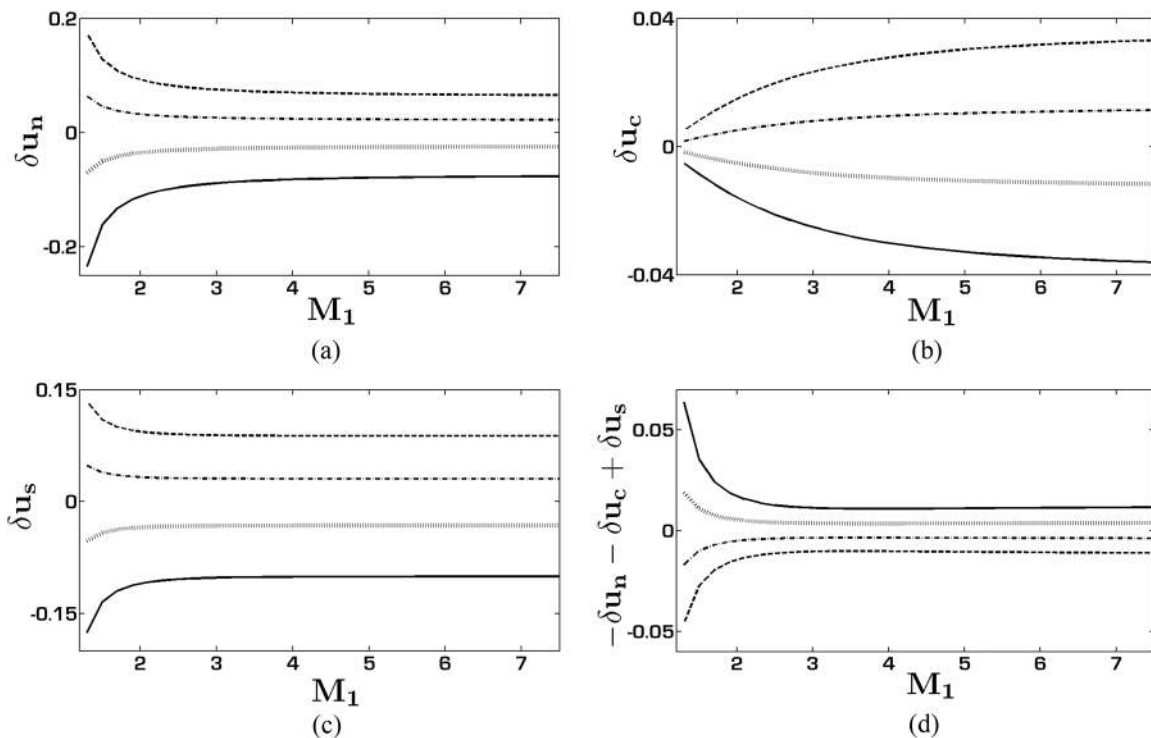

FIG. 6. Variation of various terms in Eq. (5). Each line represents a value of ε. Solid line (—): −0.06, dotted line ($\cdots$): −0.02, dashed-dotted line (–·–·–): 0.02, and dashed line (- - -): 0.06. (a) δu_n. (b) δu_c. (c) δu_s. (d) Variation of the resultant of δu terms.

in Subsection IV E and it is followed by Subsection IV F on upstream perturbations.

E. Downstream perturbations

Consider the case of a downstream perturbation with $\phi_o = 0$ approaching a stationary shock at low M_1. As seen in Fig. 6, at low M_1, the effect of the contact surface is negligible and therefore Eq. (5) can be approximated to

$$\Delta t(\phi_i) = \Delta t_o [1 + \delta x_n(\phi_{i-1}) - \delta u_n(\phi_i) + \delta u_s(\phi_{i-1})]. \quad (14)$$

For $0 < \phi < 0.5\pi$, we know that $\delta u_s > 0$, $\delta u_n > 0$, and $\delta x_n < 0$. Therefore, $\Delta t|_{pseudo\ shock} < \Delta t < \Delta t_o$ and thus we have $\hat{T}(0.5\pi) < t(0.5\pi) < 0.25\bar{T}$. For $\phi = \pi$, as nonlinear propagation terms cancel each other over a half cycle,

$$t(\phi = \pi) = 0.5\bar{T} + \sum_{j=1}^{\phi_j=\pi} \delta u_s(\phi_{j-1})\Delta t_o. \quad (15)$$

As $\delta u_s > 0$ for all $0 < \phi < \pi$, $t(\phi = \pi) > \hat{T}(\phi = \pi) = 0.5\bar{T}$.

Extending similar arguments and analysis to the negative half cycle ($\phi \in (\pi, 2\pi)$), we get $0.75\bar{T} < \hat{T}(1.5\pi) < t(1.5\pi)$. We know that u_s is purely a function of P' and P' is sinusoidal in phase. Hence, $u_s(\phi) = -u_s(\phi + \pi)$ and thus we get $t(2\pi) = \hat{T}(2\pi) = \bar{T}$. Therefore, as the shock responds for a longer time to the positive half cycle, the shock moves upstream for a longer duration than downstream. Therefore, in response to the full cycle, the shock gets displaced upstream.

1. Effect of M_1

At high upstream Mach numbers, as seen in Fig. 6, the effect of the contact surface becomes important and, hence, all the terms in Eq. (5) are to be considered. It can be seen that the difference between the δu_n and δu_s terms asymptotes to a constant value of 0.035 (approx.) for large Mach numbers. On the other hand, the δu_c term is of the order of 0.04 at high Mach numbers and is very low at low Mach numbers. Hence,

the contact surface is an indispensable flow feature to capture the shock response correctly. Figure 6(d) shows that as the Mach number increases, the net effect of δu terms decreases in magnitude but the sign remains same. This residual component of δu terms is, however, offset by δx_c. From Eq. (9), it can be seen that the magnitude of δx_n decreases with M_1, while the δx_c increases asymptotically in M_1 [Eq. (12)]. Therefore, the net departure from the sinusoidal response decreases, and the response (say pressure just downstream of shock) as a function of time will tend toward a sinusoidal profile at high Mach numbers. The nonlinear propagation and shock movement effects are varying only in the range of $M < 3$ and above this, there is only a fixed effect. Thus in the range of $M > 3$, the effect of the contact surface could not be ignored as it determines the magnitude and direction of shock drift.

2. Dependence on starting phase (ϕ_o)

By extending arguments made for the case of $\phi_o = 0$, the response of shock to sinusoidal perturbation for various starting phases can be obtained. Figure 7 shows the results for $\phi_o = 0$, 0.5π, π, and 1.5π. From this analysis, it can be seen that the effect of the starting phase and thus the history of perturbation is very important. It confirms the arguments made in Sec. III that the terms in Eq. (5) are both cumulative and local nonlinearities of the system.

3. Effect of ω and ε

Figure 8 shows that the variation of ε only scales $O(\varepsilon)$ terms and does not contain new physics. Hence, the shock response is predicted to follow the same trend, but the magnitude of response (i.e., the various inequalities) becomes more pronounced at higher ε and thus the departure of the response from the sinusoid profile becomes higher.

As all the δu terms are dependent only on the phase (ϕ), they are independent of the distance between each wave for a sinusoidal perturbation profile. Hence, the effect of ω is felt
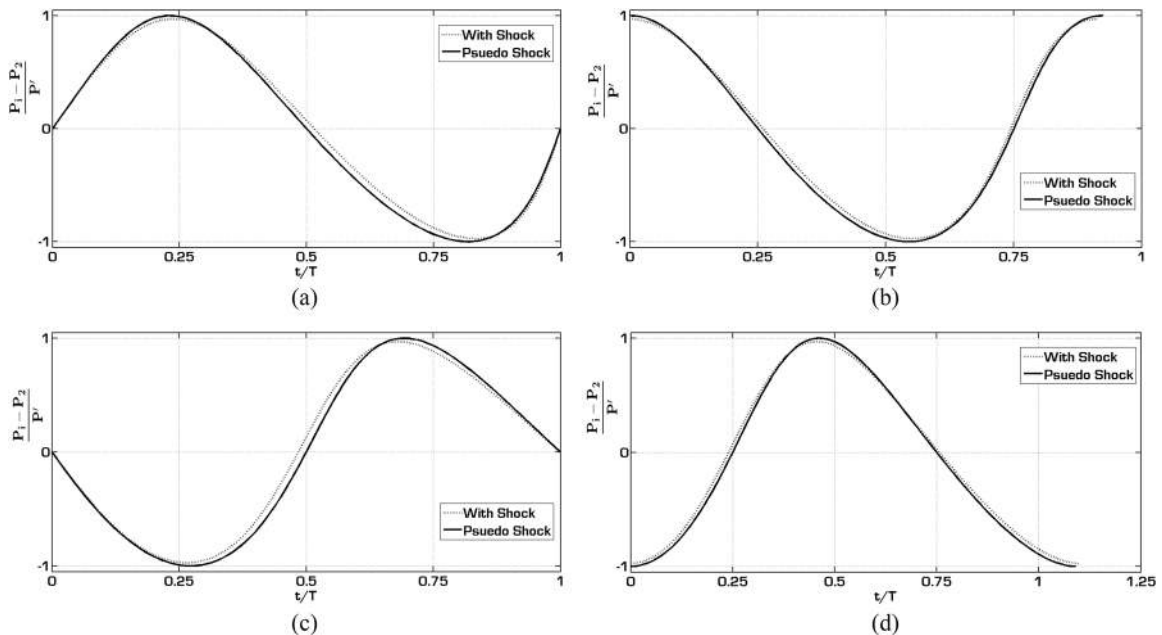

FIG. 7. Pressure downstream of shock/pseudo-shock due to downstream perturbation for different ϕ_0. (a) $\phi_o = 0$. (b) $\phi_o = 0.5\pi$. (c) $\phi_o = 1.0\pi$. (d) $\phi_o = 1.5\pi$.
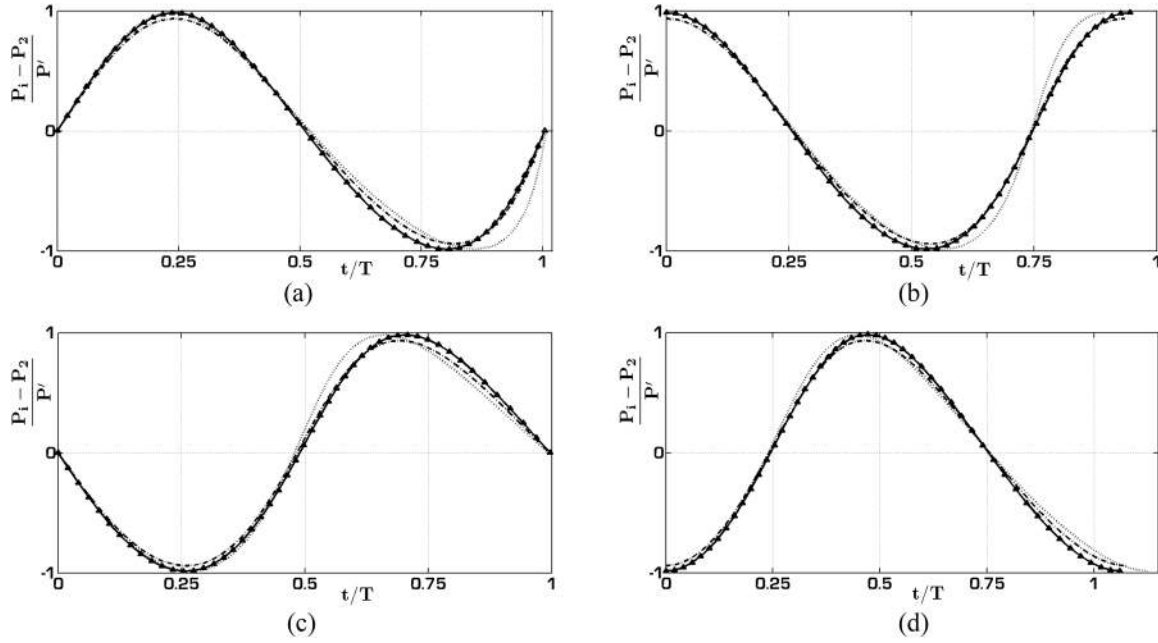
FIG. 8. Variation of downstream pressure experienced by the shock with time due to downstream perturbations. The plot is to be read as follows: triangular marker ($\triangle$) for $M_1 = 1.5$, $\varepsilon = 0.02$, $\omega = 10$ Hz; solid line (—) for $M_1 = 1.5$, $\varepsilon = 0.02$, $\omega = 100$ Hz; dotted line ($\cdots$) for $M_1 = 1.5$, $\varepsilon = 0.04$, $\omega = 100$ Hz and dashed-dotted line ($-\cdot-\cdot-$) for $M_1 = 2.5$, $\varepsilon = 0.04$, $\omega = 100$ Hz. (a) $\phi_o = 0$. (b) $\phi_o = 0.5\pi$. (c) $\phi_o = 1.0\pi$. (d) $\phi_o = 1.5\pi$.

only through the quantity Δt_o. Also, δx terms scale linearly with δu terms and though they are dependent on the history of perturbation, only the relative positioning of each wave is important. Therefore, the frequency of perturbation has only a scaling effect on the shock response and becomes independent of it when $t(\phi)$ is scaled with the time period of the perturbation ($\bar{T}$).

F. Upstream perturbations

In the case of upstream perturbations, the effect of the contact surface does not exist because the contact surfaces are convected downstream along with the flow while the perturbation waves exist only upstream of shock. Hence, the response is predicted by Eq. (14). From Fig. 2, we see that the effect of nonlinearity is negligible in the case of upstream perturbation. This can be deduced by the non-dimensional term δu_s which has been defined as the ratio of the speed of the shock to the speed of propagation of the wave. Now, while the shock speed, being a function of the pressure jump across the shock, is similar for both the downstream and upstream perturbation, the speed of wave propagation is larger for the upstream perturbation compared to its downstream counterpart for the same frequency of perturbation. This makes δu_s much smaller for the case of an upstream perturbation than for the case of a downstream perturbation. Hence, all the nonlinear effects become negligible and therefore, the response of the shock will be a sinusoid for upstream perturbations. By similar arguments, the ratio of amplitude of shock oscillation to the wavelength of perturbation is an order of magnitude less than the corresponding downstream perturbation value.

If the response of shock to upstream perturbation is plotted similar to the downstream perturbation (Fig. 7), it would be a sinusoid in time shifted according to the initial phase of the perturbation, ϕ_o. As in the case of downstream

perturbations, ε and ω scale the response because they do not contain new physics as the response is purely a sinusoid. Note that in the case of upstream perturbation, the change in pressure gets amplified across the shock. Therefore, the magnitudes of maxima and minima of the ratio to be plotted along the y-axis is always greater than 1. As M_1 increases, this amplification increases and therefore the magnitudes of maxima and minima increase. We know that

$$M_s = M_1 - \sqrt{\frac{\gamma + 1}{2\gamma}\left(\frac{P_2}{P_1} - 1\right) + 1}, \qquad (16)$$

where M_s is the Mach number of the shock. So, the velocity of shock is purely a function of the pressure ratio across the shock. For an upstream perturbation, this ratio is altered by varying the denominator. Thus the magnitude of minima of pressure ratio is higher than that of maxima, unlike the downstream case, where the numerator is varied and thus the magnitude of maxima and minima are same. Therefore, the magnitude of velocity of the shock is higher for the negative half cycle than the positive half cycle (i.e., the magnitude of shock velocity in the upstream direction is higher than that in the downstream direction). This coupled with the prediction that duty cycles of positive and negative half cycles are equal results in a net upstream motion of shock over one full sinusoidal cycle of perturbation for any upstream perturbation.

V. WAVE TRACKING STUDY

A. Algorithm

The given perturbation profile is discretized to a finite number of waves. This number of waves, n, is chosen such that the shock response is same (i.e., difference is less than 0.1% variation in the time period of shock response) for $n/2$ and $2n$ number of waves (typically $n = 100$). The first wave reaches the

shock and generates a contact surface and a residual wave. The contact surface is tracked till it interacts with all the remaining upstream traveling waves. At each shock-wave interaction and contact surface-wave interaction, the position and new propagation speed of the waves are obtained by solving a Riemann problem. As seen in Sec. III B, the residual wave is insignificant with respect to the contact surface and is therefore not tracked. The method to solve the Riemann problem is same as the one discussed in Sec. III B. The waves travel upstream with the new speeds till they encounter a contact surface or shock. The computations are essentially performed by tracking each contact surface (initially formed due to shock-wave interaction) till it interacts with all remaining waves (the jump across the contact surface changes after each interaction). This method of tracking the waves has been verified by calculating various standard flow fields like a piston moving into a quiescent flow, shock tube, etc. Apart from the approximation of neglecting residual wave, this study is exact. The approximation of neglecting the residual wave results in a very low error at low supersonic Mach numbers. In the case of upstream perturbations, as the contact surface and residual wave do not interact with waves approaching the shock, this analysis becomes exact at any Mach number. This method is different from the CFD method used in Sec. VI where a control volume (stationary) approach is used to solve the Euler equations in the integral form.

B. Observations

From Fig. 8, it can be seen that the predictions made in Secs. III and IV regarding shock response are verified. The perturbation frequency ω indeed has a purely scaling effect. Furthermore, as ε increases, the departure from the sinusoidal response increases and the response tends toward a sinusoid in time as M_1 increases. Also, it can be concluded that the response of shock to perturbation has a cumulative nonlinearity and, therefore, the history of perturbation plays an important role.

However, small departures do exist and could be because of the $O(\varepsilon^2)$ and higher order terms. In Fig. 8, for $\phi_o = 0°$, it is seen that $t(2\pi) > \bar{T}$ but the analytical study predicts that $t = \bar{T}$. This could be because of the additional distance the waves need to travel due to the upstream movement of the shock that

has been neglected in the analytical treatment as it is a higher order effect. From similar arguments, it can be seen that for $\phi_o = 180°$, $t(2\pi + \phi_o) < \bar{T}$. However, these effects were shown to be higher order effects and neglected by analytical predictions and hence these small departures from the predictions are observed and are to be expected.

As predicted by the analytical study, the response is seen not to be a sinusoid and, therefore, it is not obvious if the shock will return to its initial position. This difference between the final and initial shock positions after one cycle of perturbation is referred to as "drift." As the response is not sinusoidal, the amplitude of the shock location is defined as the distance between the extreme positions during one full cycle of perturbation. These variables, drift and amplitude of shock movement, are of practical consequence and, hence, the effect of various parameters on these variables is presented. Drift and amplitude of shock movement decrease with Mach number (M_1), increase with amplitude of perturbation imposed (ε), and scale linearly with wavelength (in Fig. 9, wavelength appears as a normalization factor on the vertical axis). The data presented by Moase et al.[10] support the observation that shock drifts over a full cycle of sinusoidal perturbation. However, they have neither mentioned this observation nor explained it in their study. Experimental investigations by Bruce and Babinsky[11] have not revealed any drift. This could be because, as mentioned, they have manually operated the wind tunnel valve if the mean position of shock was varying or could be due to the short length of the tunnel which would mean less nonlinearity.

The result that ω has only a scaling effect on the amplitude of the shock movement has been verified experimentally[11] and similar result was obtained through previous analytical studies.[1,2] It is important to note that though the analytical study predicted the variation of shock response and thus the sign of drift for a given ϕ_o, it could not predict further details of the variation across ϕ_o as it necessitates the use of higher order terms, and hence only a wave tracking numerical study is performed to analyze the effect of ϕ_o.

For the case of upstream perturbations, as predicted, the response is independent of ϕ_o, the amplitude of the response (variation of downstream pressure normalized by the amplitude of upstream perturbation) increases with M_1, and ε and ω have a scaling effect, as seen in Fig. 10. The wave tracking study shows that the response is not exactly a sinusoid
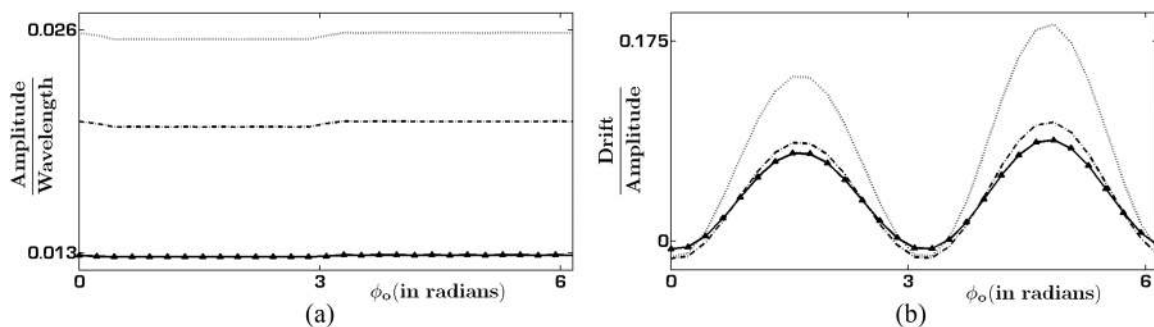

FIG. 9. Variation of amplitude of shock movement and drift with various flow parameters due to downstream perturbations. The plot is to be read as follows: triangular marker ($\triangle$) for $M_1 = 1.5$, $\varepsilon = 0.02$, $\omega = 10$ Hz; solid line (—) for $M_1 = 1.5$, $\varepsilon = 0.02$, $\omega = 100$ Hz; dotted line ($\cdots$) for $M_1 = 1.5$, $\varepsilon = 0.04$, $\omega = 100$ Hz and dashed-dotted line ($-\cdot-\cdot-$) for $M_1 = 2.5$, $\varepsilon = 0.04$, $\omega = 100$ Hz. (a) Amplitude. (b) Drift.
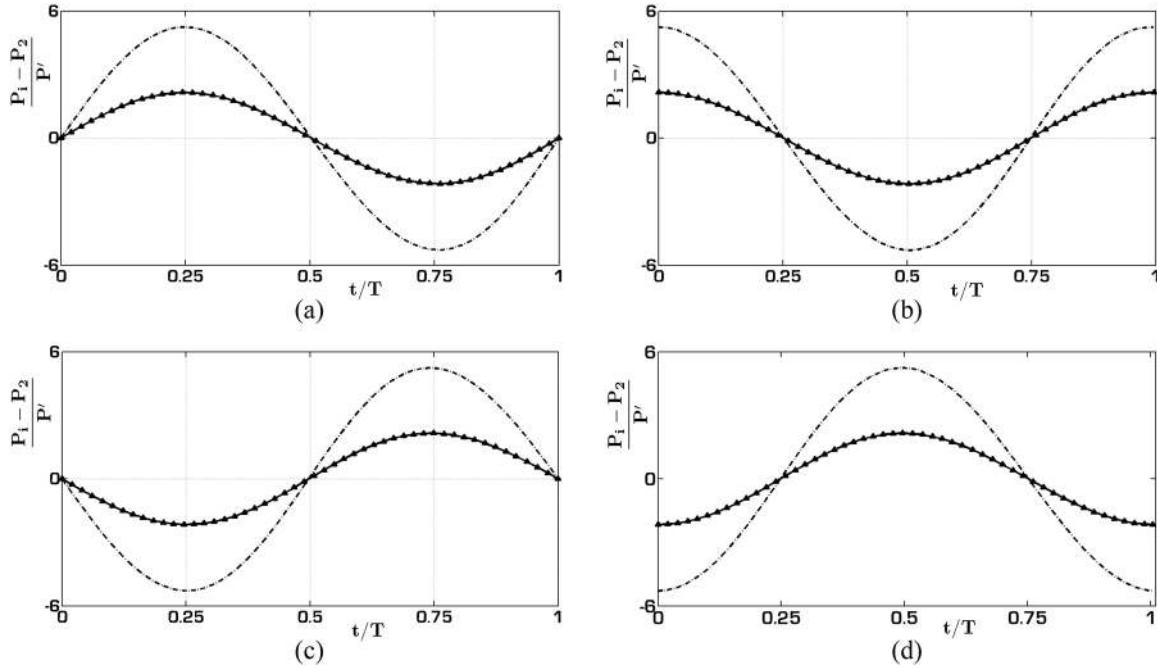
FIG. 10. Variation of downstream pressure experienced by the shock with time due to upstream perturbation. The plot is to be read as follows: triangular marker ($\triangle$) for $M_1 = 1.5$, $\varepsilon = 0.02$, $\omega = 10$ Hz; solid line (—) for $M_1 = 1.5$, $\varepsilon = 0.02$, $\omega = 100$ Hz; dotted line ($\cdots$) for $M_1 = 1.5$, $\varepsilon = 0.04$, $\omega = 100$ Hz and dashed-dotted line ($-\cdot-\cdot-$) for $M_1 = 2.5$, $\varepsilon = 0.04$, $\omega = 100$ Hz. (a) $\phi_o = 0$. (b) $\phi_o = 0.5\pi$. (c) $\phi_o = 1.0\pi$. (d) $\phi_o = 1.5\pi$.

(too small to be visible directly from Fig. 10). This departure (about 0.5% variation in the duty cycle) is to be expected as we have neglected the nonlinearities for the analytical studies as they were small. Nevertheless these small effects are captured by the wave tracking study as it is exact. The amplitude of the shock movement, as predicted analytically, is much smaller than the corresponding downstream cases {compare the magnitude of amplitude for upstream perturbations [Fig. 11(a)] with that corresponding to downstream perturbations [Fig. 9(a)]}. The drift too, as predicted, is always in the upstream direction for all conditions of flow and perturbations [Fig. 11(b)].

Hence, it can be seen that overall there is a very good match between the analytical predictions and wave tracking results. In the semi-analytical wave tracking method, the weak residual waves which are resultant of the shock-perturbation

interaction are neglected. It was further assumed that the contact surface, when interacting with the next downstream (incoming) perturbation, only alters the speed of the perturbations and produces a downstream contact surface, but does not create any other waves. This is not true, as there will always be a weak residual wave created in each of these interactions. These weak waves were neglected in the semi-analytical wave tracking simulation as it was very expensive to keep track of the huge number of waves generated by each such interaction and follow their interactions with other waves in the flow. It is possible that there are cumulative effects here, which are lost when neglecting these weak waves, in the semi-analytical method. By contrast, a CFD simulation does not make any such assumption. Thus, CFD simulations of the same problem were performed and results are compared with the results from the wave tracking methods in Sec. VI.
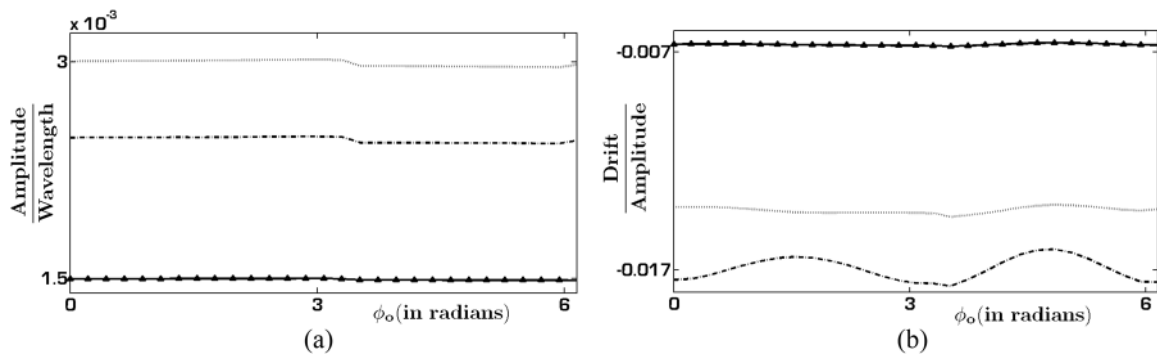

FIG. 11. Variation of amplitude of shock movement and drift with various flow parameters for upstream perturbations. The plot is to be read as follows: triangular marker ($\triangle$) for $M_1 = 1.5$, $\varepsilon = 0.02$, $\omega = 10$ Hz; solid line (—) for $M_1 = 1.5$, $\varepsilon = 0.02$, $\omega = 100$ Hz; dotted line ($\cdots$) for $M_1 = 1.5$, $\varepsilon = 0.04$, $\omega = 100$ Hz and dashed-dotted line ($-\cdot-\cdot-$) for $M_1 = 2.5$, $\varepsilon = 0.04$, $\omega = 100$ Hz. (a) Amplitude. (b) Drift.
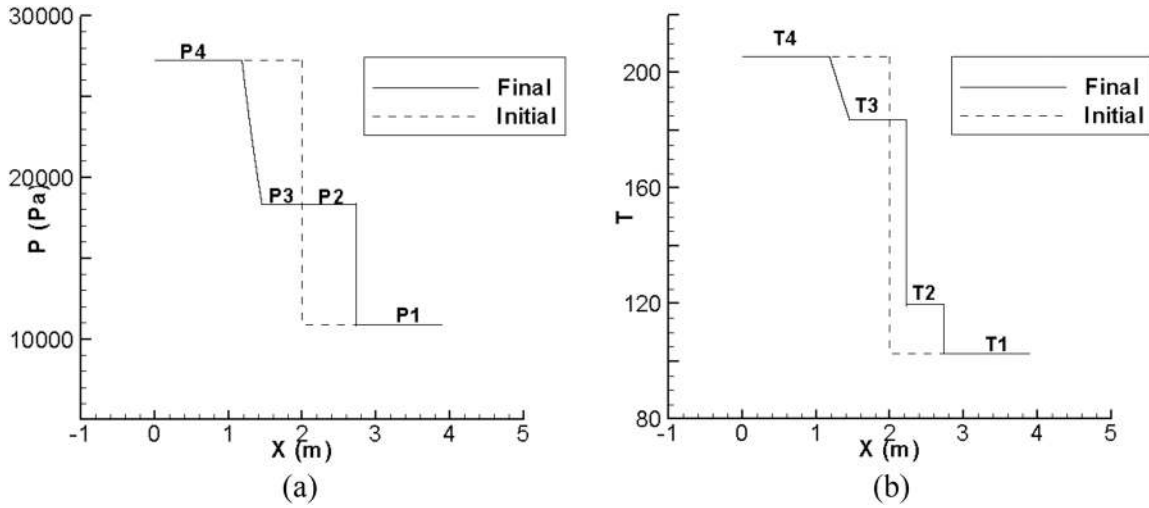
FIG. 12. Distribution of pressure and temperature for a shock tube simulation; initial conditions P4 = 27 240.6 Pa, P1 = 10 896.2 Pa; T4 = 205.6 K, T1 = 102.8 K are shown by the dotted lines. (a) Pressure. (b) Temperature.

VI. CFD SIMULATION

A. Validation

CFD simulations are performed to compare with the predictions of the semi-analytical and analytical work presented earlier in this paper. The code used for simulation of the shock-perturbation interaction performed in this work is a finite volume based solver for the discretized Euler equations. The Low Diffusion Flux Splitting Scheme (LDFSS)[15] is used for the first order reconstruction of interface fluxes using the left and right states (reconstructed) at the interface using the 4th piecewise parabolic method.[16] The equations are integrated in time using a 4th order CFD type Runge-Kutta scheme. A global time stepping with a CFL number of 1.0 is used here.

The 1-D Euler code is validated by simulating a shock tube case. Figure 12 shows the jump in the pressure and temperature for the shock-tube simulation. The domain for this simulation extends from $X = 0$ to $X = 20$ m. A spacing of $\delta = 0.5 \times 10^{-4}$ m is used for this simulation. The shock tube simulation is initiated as a Riemann problem at $X = 2.0$ m, with discontinuities in pressure, density, and temperature. This is shown in Fig. 12, where the left state is denoted by "4" and the right state by "1." The choice of the left and right states are *ad hoc*. The given initial condition would generate a right moving shock, an expansion wave moving to the left, and a right moving contact discontinuity in between. Figure 12 also shows the comparison of the pressure and temperature distributions initially and after 20 000 iterations. The plot of pressure in Fig. 12(a) shows the presence of a region of expansion followed by a discontinuity across the moving normal shock. In Fig. 12(b), in addition to the changes in temperature across the expansion fan and the normal shock, a strong jump is observed across the moving contact surface, which is located between the expansion and normal shock. To get an estimate of the error in the predictions of the CFD code, a comparison of flow properties determined analytically and those computed by the simulation are presented in Table I after 20 000 iterations.

A plot of the shock location vs time for 20 000 iterations is also shown in Fig. 13. As can be seen in this plot,

the shock position determined analytically and that predicted by the simulation virtually coincide.

In addition to the shock-tube simulation, a slow moving shock[17] is also simulated to validate the solver. This is included to check whether downstream-running noise of large wavelength and/or amplitude, as observed with the use of Roe's flux-difference splitting scheme,[17] are also generated with the present solver, which employs a flux-vector splitting scheme. It is especially important in this case to determine if the pressure downstream of the moving shock shows any discernible noise, as it would raise doubts about the accuracy of CFD predictions of the pressure field (downstream) due to the shock-perturbation interaction studied in this work.

The computational domain for this case, which extends from $X = 0$ m to $X = 2$ m, consists of 200 cells of equal

TABLE I. Comparison between analytical and computational solutions.

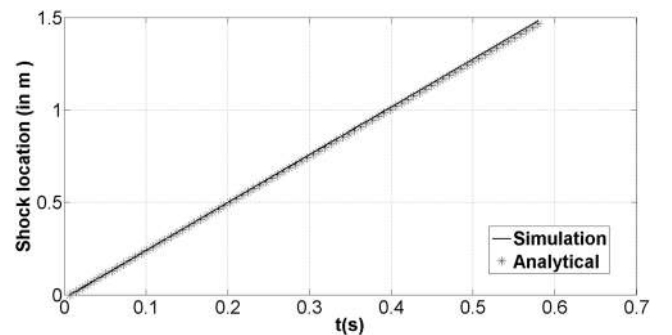| Property	Analytical	Simulation	Error (%)
T2	119.3 K	119.8 K	0.4
P2	18631 Pa	18351 Pa	1.5
T3	183 K	183.7 K	0.4
P3	18631 Pa	18351 Pa	1.5
Up (induced flow)	78.74 m/s	79.72 m/s	1.2

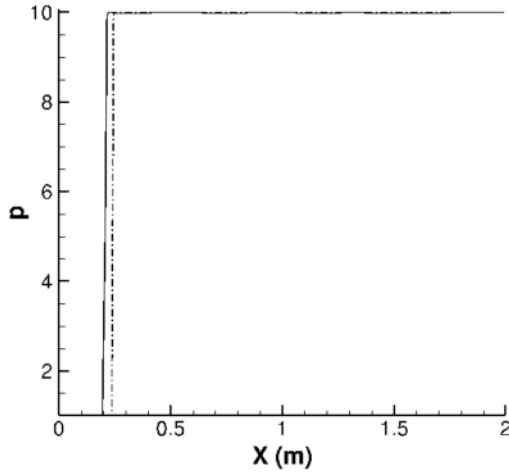FIG. 13. Shock location history for the shock-tube simulation.

FIG. 14. Normalised pressure vs. X for a slow left-moving shock; dashed-dotted line: initial shock, solid line: after 1.8 ms.
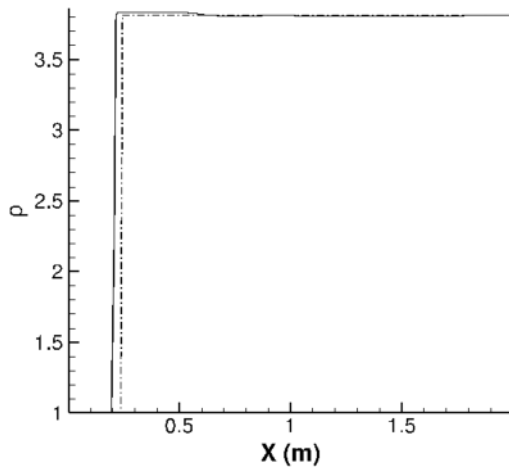

FIG. 15. Normalised density vs. X for a slow left-moving shock; dashed-dotted line: initial shock, solid line: after 1.8 ms.

size. The jumps in thermodynamic properties satisfying the Rankine-Hugoniot condition, which corresponds to a Mach number of ≈ 2.95, is imposed at $X = 0.25$ m. A supersonic

inflow boundary condition is used at $X = 0$ m and a subsonic outflow (fixed pressure) boundary condition is used at $X = 2$ m. The flow speeds to the left and right of the discontinuity are calculated to ensure a left-moving shock at low speed; the ratio of the shock speed (left moving) to the fastest wave speed in the flow is ≈ 66.95. The simulation is run for a total time of about 1.8 ms, during which the shock moves upstream by 0.024 m. Figure 14 shows the variation in pressure (normalised by the values left of the shock) with distance. It can be observed that the pressure downstream of the shock remains practically unaltered due to the shock movement and as such, any right (downstream) running acoustic waves (if present downstream of the shock) are too small to be visible at this scale. Figure 15, however, shows minor differences in the density across the stationary and moving shocks, indicating that the solver (flux-splitting scheme specifically) is giving rise to right-moving entropy waves; the amplitude of these waves though appear to be small ($\approx$less than 1% of the downstream density).

Based on the above validations, it can be stated the Euler solver used in this work is capable of predicting 1-D flowfields with good accuracy and also does not introduce large-amplitude noise downstream of moving shocks and as such is used for the rest of the CFD results presented here.

B. Computational domain and introduction of perturbation

The computational domain for the shock-perturbation studies extends from $X = -2\lambda$ to $X = 8\lambda$, where λ is the wavelength of the perturbation. To study the effect of a downstream wavelet on the shock, a sinusoidal perturbation is introduced right at the shock location. In the computational domain, the shock is located at a distance of 2 times the wavelength of the perturbation from the origin. Figure 16(a) shows the position of the perturbation downstream of the shock for two different values of ϕ_o. The initial amplitude of the perturbation is chosen as twice the amplitude of the wave since it splits into a left and a right running wave, of which only the left running
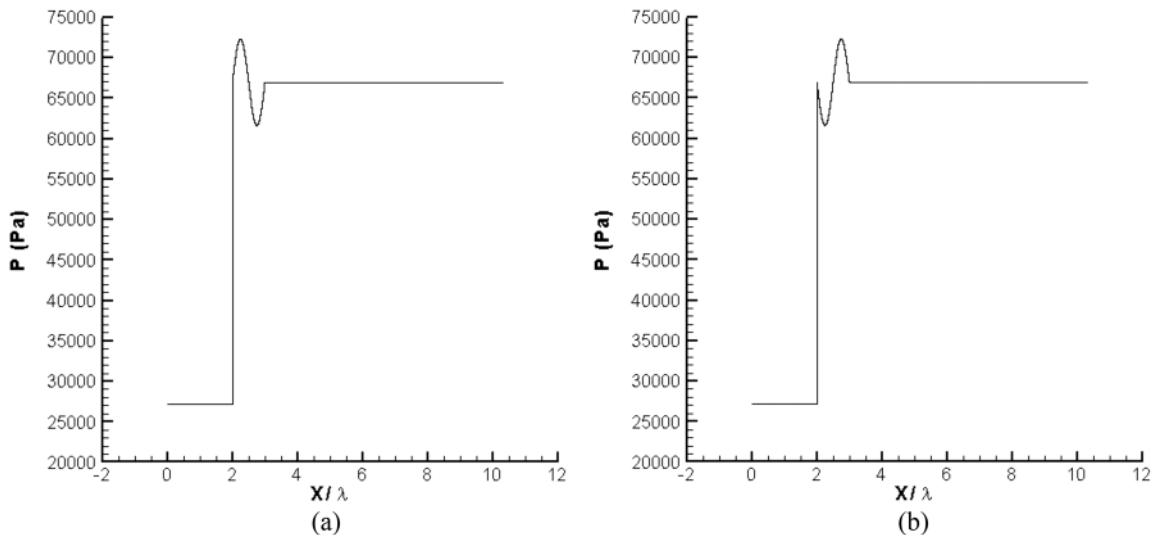

FIG. 16. Variation of pressure in the computational domain at t = 0 for $M_1 = 1.5$ and $\epsilon = 0.04$. (a) $\phi_o = 0$. (b) $\phi_o = \Pi$.

TABLE II. Comparison of errors for different grid resolutions.

Resolution ($\frac{ncells}{\lambda}$)	Drift (m)	$\frac{drift}{\Delta x}$	Error (%)
10 000	-9.98×10^{-5}	1	20.16
20 000	-1.25×10^{-4}	2.5	≈ 0
40 000	-1.25×10^{-4}	5	...

wave interacts with the shock. The thermodynamic properties of the perturbed state are constructed assuming isentropic processes of compression and expansion from the post-shock state to the perturbed state. In this context, it is different from the semi-analytical simulations presented earlier, wherein the perturbations are modelled as weak compression and expansion shocks. The velocities at the perturbed state are kept the same as the post-shock state. This means that while local total enthalpy at any point in the perturbed state may be different from the post-shock state (at the same point), there is no global energy addition to the system. The length of the computational domain to the right of the shock is 8 times the perturbation wavelength (λ). A much larger length (compared to upstream of shock) is chosen for the downstream direction to ensure that any wave formed due to the interaction of the right moving wave with the right boundary does not travel upstream and interact with the shock or left moving wave within the time frame of the simulation.

As the code uses a density based solver, the perturbation is introduced by setting the temperature and density values in order to cause the desired pressure change using an assumption of isentropic process.

C. Grid refinement and CFL study

The grid spacing for this work is expressed using the metric number of grid points per unit wavelength of the perturbation. The wavelength (λ) of the perturbation is defined as $\frac{wavespeed}{frequency}$, where wave speed is the acoustic velocity after the shock and the frequency is 100 Hz. The perturbation amplitude (ϵ) was taken as 0.04 for these simulations. Three different grid spacings have been tried as listed in Table II. Based on the values of drift obtained for the different grids, a resolution of 40 000 $\frac{cells}{\lambda}$ is used for all the simulations at $M = 1.5$. This results in a physical spacing of $\Delta X = 2.4953 \times 10^{-5}$ m. The use

of the quantity $\frac{ncells}{\lambda}$ to determine the grid resolution ensures that the grid spacing is problem specific.

As seen from Table II, the highest grid resolution considered corresponds to a drift of -1.25×10^{-4} m. This is assumed to be closest to the true value. Thus the errors are calculated with respect to this value and are tabulated. Although a grid resolution of 20 000 $\frac{cells}{\lambda}$ shows similar value of drift as for the finest mesh, the finest mesh is used for all the subsequent CFD studies, as for smaller values of perturbation amplitude ($\epsilon = 0.03$), the lower resolution cannot capture the drift.

To check for the sensitivity of the solution to the CFL number, the simulation for $M = 1.5$, $\epsilon = 0.04$, and a frequency of 100 Hz was run at two different CFL numbers of 0.5 and 1.0. The results show hardly any difference (not shown here). As such, a CFL of 1.0 has been used for the rest of the simulations presented here.

To reduce the number of cells in the domain, instead of using a uniform grid for the entire domain, only a part of the domain from X = 0 to X = 3λ has a constant grid spacing, beyond which a stretched grid is used with a constant stretching ratio of 4%. The grid-resolution mentioned earlier pertains to the uniform grid from X = 0 to X = 3λ.

D. Results

The simulation results from the shock-perturbation simulations have been plotted against the results obtained from the previously discussed semi-analytical algorithm (Sec. V) for specific cases. If the final position of the shock is upstream of the initial position (upstream drift), then the drift is taken as negative.

Figure 17 plots change in the pressure just downstream of the shock, due to the interaction with the perturbation, normalized by the magnitude of the perturbation, vs the non-dimensional time t/T as defined before. From Fig. 17, it is observed that the downstream pressure variation predicted by the semi-analytical method and the CFD simulation match very closely for phase angles $\phi_o = 0$ and π. Some noise in the pressure data is observed and this can be attributed to post shock oscillation in pressure across a moving shock observed in most higher order numerical methods. Figure 18 shows that the shock movement predicted by the semi-analytical method and the CFD simulation match very closely as well.

Figure 19(a) compares CFD predictions of the amplitude of shock motion with those computed using the semi-analytical
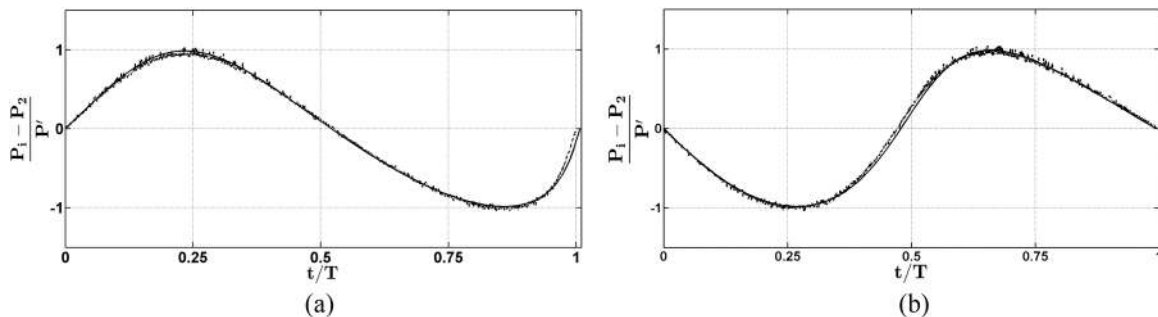

FIG. 17. Variation of downstream pressure experienced by the shock with time due to a downstream perturbation; $M_1 = 1.5$, $\varepsilon = 0.04$, $\omega = 100$ Hz; solid line (——): semi-analytical method, dashed-dotted line (– · – · –): CFD simulation. (a) $\phi_o = 0$. (b) $\phi_o = \Pi$.
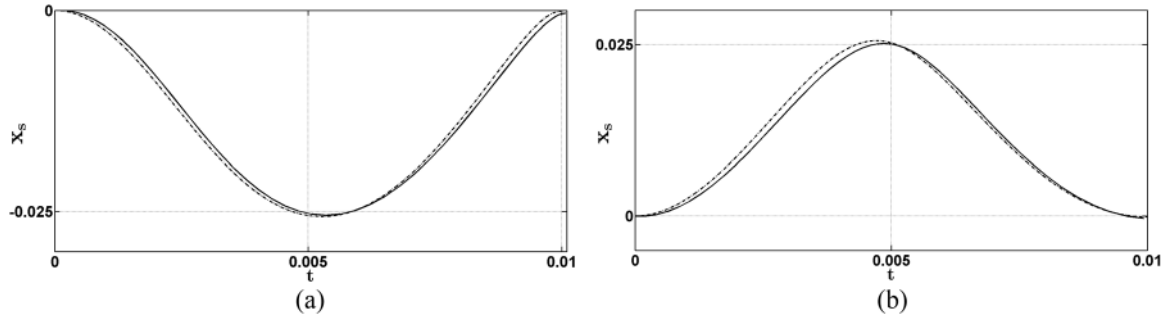
FIG. 18. Variation of shock location with time due to a downstream perturbation; $M_1 = 1.5$, $\varepsilon = 0.04$, $\omega = 100$ Hz; solid line (—): semi-analytical method, dashed-dotted line ($-\cdot-\cdot-$): CFD simulation. (a) $\phi_o = 0$. (b) $\phi_o = \Pi$.
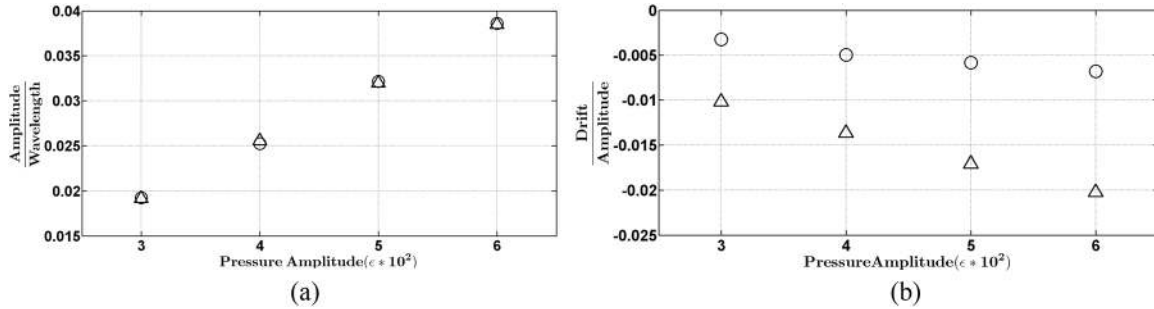

FIG. 19. Comparison of amplitude of shock movement and drift between the semi-analytical method and the CFD simulation. $M_1 = 1.5$, $\omega = 100$ Hz; triangle marker (Δ): semi-analytical method; circle (o): CFD solution. (a) Amplitude. (b) Drift.

method, at discrete values of perturbation amplitude at Mach 1.5. As shown in the plot, the computational results almost match the semi-analytical method. Figure 19(b) shows a comparison of drift values obtained from CFD computations and the semi-analytical method, at the same set of perturbation amplitudes used in Fig. 19(a) at Mach 1.5. As observed, the drift values predicted by the CFD methods are lower compared to their semi-analytical results. However, the two sets of results agree qualitatively in the sense that both show a similar direction of drift and a growth in the drift as the amplitude of perturbation increases.

Figure 20 compares the CFD predictions of pressure downstream of the shock, and the shock motion, with the results from the semi-analytical method, for two successive perturbations for a Mach 2.5 flow at a perturbation

amplitude of 4%. Similar to what was observed for the case of a single perturbation, the two methods compare very well in this case also. Table III lists the values of drift as computed using CFD, and the semi-analytical method, for 1, 2, and 3 perturbations at a perturbation pressure amplitude of 4% and Mach 1.5 flow. Here the results of the semi-analytical method suggest that the drift scales linearly with increase in the number of perturbations. The CFD predictions of drift also increase with successive perturbations, although the magnitude of change is less compared to the semi-analytical method.

The CFD results show a good level of agreement with the semi-analytical method in general, except in the prediction of drift, where the CFD results are consistently lower compared to those obtained from the semi-analytical method. This can
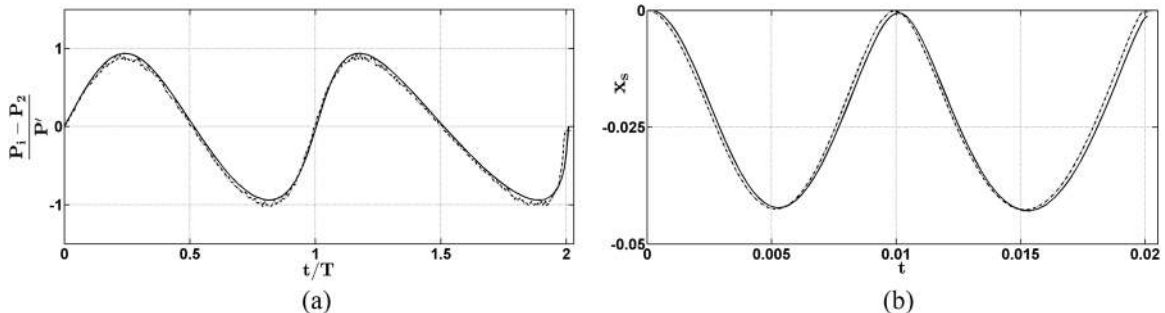

FIG. 20. Variation of downstream pressure and shock location with time for two successive perturbations; $M_1 = 2.5$, $\varepsilon = 0.04$, $\omega = 100$ Hz, $\phi_o = 0$; solid line (—): semi-analytical method, dashed-dotted line ($-\cdot-\cdot-$): CFD simulation. (a) Downstream pressure variation. (b) Shock movement.

TABLE III. Comparison of drift values (in m).

No. of perturbations	Semi-analytical method	CFD method
1	-6.39×10^{-4}	-2.07×10^{-4}
2	-1.3×10^{-3}	-3.62×10^{-4}
3	-1.9×10^{-3}	-5.69×10^{-4}

primarily be attributed to the minor phase difference in the response of the shock to the perturbation between the two methods as can be seen in Fig. 18.

VII. CONCLUSIONS

This study investigated the response of a normal shock in a constant area duct to sinusoidal perturbations. In this interaction, the contact surface, which was ignored by researchers in previous studies, is shown to have a significant effect on the flow field downstream of shock and consequently the shock response to downstream disturbances. For upstream perturbations, however, the interaction is important only to determine the downstream pressure and the shock velocity. In this case, the contact surface and residual wave generated in the process are not important, as they exist only in the flow field downstream of shock, which is devoid of any externally imposed perturbation.

It is demonstrated both analytically and numerically that the shock responds nonlinearly to perturbation and the nonlinearity is both cumulative and local in nature. Hence, a linear superposition of sinusoidal waves to simulate a complicated perturbation profile may not work. Furthermore, the shock response depends strongly on the perturbation history (ϕ_o). The nonlinear nature of the response can be further seen by the change in the time period of shock response with respect to the time period imposed by the perturbation. In addition to this variation, the duty cycle of positive and negative half cycles of perturbation is altered. This results in a net upstream displacement of the shock over one full cycle of perturbation, which is referred to as drift. Although the magnitude of drift scales with Mach number, $\frac{drift}{amplitude}$ is higher for lower Mach numbers. This suggests that the effect of drift is more pronounced at low supersonic Mach numbers. This observation may have practical consequences, as this is the typical operating regime for ramjets. Further studies are underway to examine the effect of geometric variations, such as a C-D nozzle, on this nonlinear response of shock.

In the case of upstream perturbations, the duty cycle is very close to that of a sinusoid, as the nonlinearities are very small. However, the magnitude of shock velocity, being lower for the positive half cycle than the negative half cycle, causes the shock to drift upstream over one full cycle of perturbation. Thus we see that a shock does not come back to its initial position, but ends up more upstream, for both upstream and downstream sinusoidal perturbations. Furthermore, multiple waves interacting with the shock result in a cumulative effect on the shock movement.

In summary, this work studied in detail the interactions between various flow features (shock-wave, contact surface-wave) in a normal shock/perturbation interaction. It

conclusively establishes the shock response to be nonlinear and that the shock does not return to its initial position over one full cycle. Various physical processes behind the nonlinearities were investigated thoroughly, and the parametric variation of drift was explained. The drift in shock discussed in this study is caused solely because of the unsteady perturbation. This, coupled with geometric variation and spatial reflection of waves, could lead to sustained oscillations. Further investigations are underway to verify this possibility.

APPENDIX: SHOCK RESPONSE (ANALYTICAL FORM)

As seen in Sec. II A, each wave in the perturbation travels at a different speed. Therefore, each wave has a non-zero relative velocity with respect to its neighboring wave and, hence, the distance between each of them gets altered. The distance altered due to this nonlinear propagation can be obtained as

$$\delta x_n = \frac{u(\phi_{i-1}) - u(\phi_i)}{\Delta x_o}[t_{initial} + t_s], \qquad (A1)$$

where $t_{initial}$ is the time taken by the $(i-1)$th wave to reach the shock position at $x_s(t = 0)$, x_s is the shock location, and t_s is the time required to reach shock at $t(\phi_{i-1})$ from $x_s(t = 0)$. It is to be noted that in writing the above expression, the observation that the contact surface alters the velocity of all the upstream traveling waves by nearly the same amount is utilized. Thus, the term $(u(\phi_{i-1}) - u(\phi_i))$ can be assumed constant in time. Rewriting temporal terms in Eq. (A1), we get

$$\delta x_n = \frac{u(\phi_{i-1}) - u(\phi_i)}{\Delta x_o} \left[\frac{x(\phi_{i-1})|_{t=0}}{u_{avg}(\phi_{i-1})} + \frac{x_s|_{t=t(\phi_{i-1})}}{u_{avg}(\phi_{i-1})} \right], \quad (A2)$$

where $u_{avg}(\phi_{i-1})$ is the average velocity of the ith wave over the time $t(\phi_i)$. Substituting Eq. (5) in Eq. (2), we get

$$t(\phi_i) = \hat{T}(\phi_i)[1 + \delta] = (x(\phi_i)/u_0)[1 + \delta], \qquad (A3)$$

where $\hat{T}(\phi_i)$ is the time taken by the ith wave to reach $x(\phi_1)|_{t=0}$ in the case of the linearly propagating wave in the absence of shock and δ is the contribution of $\mathcal{O}(\varepsilon)$ terms. As the waves are uniformly spaced, Eq. (A3) can be written as

$$t(\phi_i) = i\Delta t_o(1 + \delta). \qquad (A4)$$

Substituting Eq. (A3) in Eq. (A2), we get

$$\delta x_n = \frac{u(\phi_{i-1}) - u(\phi_i)}{\Delta x_o} \frac{u_0}{u(\phi_{i-1})} \hat{T}(\phi_{i-1})$$

$$\times \left[1 + \frac{u_{s,avg}}{u_0} \frac{t(\phi_{i-1})}{\hat{T}(\phi_{i-1})} \right] \frac{u(\phi_{i-1})}{u_{avg}(\phi_{i-1})}.$$

Recall that

$$\delta u_s = \frac{u_{s,avg}}{u_0}$$

and

$$\Delta x_0 = \Delta t_0 u_0.$$

Substituting Eq. (A4) in the last expression and expanding all the individual terms in to $\mathcal{O}(\varepsilon)$, we get

$$\delta x_n \approx \left[\frac{(1 + \delta u_n(\phi_{i-1})) - (1 + \delta u_n(\phi_i))}{1 + \delta u_n(\phi_{i-1})} \right] (i - 1)$$

$$\times \left[\frac{1 + \delta u_s(1 + \delta)}{1 + \delta u'(\phi_{i-1})} \right], \tag{A5}$$

where $\delta u'(\phi_{i-1})$ is a $\mathcal{O}(\varepsilon)$ term representing the expansion of $u_{avg}(\phi_{i-1})$ about $u(\phi_{i-1})$.

Simplifying Eq. (A5) using Binomial expansion to the $\mathcal{O}(\varepsilon)$ term, we obtain

$$\delta x_n(\phi_{i-1}) \approx [\delta u_n(\phi_{i-1}) - \delta u_n(\phi_i)](i - 1) \propto max\{\delta u_n(\phi_j)\}, \tag{A6}$$

where the index $j \in 1, 2, \ldots, n$.

An important observation from this analysis is that the shock displacement terms are absent in Eq. (A6) and hence it can be concluded that shock displacement has a higher order effect on shock response. Also, through this derivation, we have obtained the functional dependence of δx_n on δu_n. Thus, the variation of δx_n with perturbation and mean flow parameters can be studied through δu_n which is dependent only on ϕ.

[1] H. G. Hurrell, NACA TN 4090, 1959.

[2] F. E. C. Culick and T. Rogers, "The response of normal shocks in diffusers," AIAA J. **21**, 1382 (1983).

[3] C. P. Chen, M. Sajben, and J. C. Kroutil, "Shock-wave oscillations in a transonic diffuser flow," AIAA J. **17**, 1076 (1979).

[4] M. Sajben, T. Bogar, and J. Kroutil, in *AIAA Conference* (AIAA, 1981).

[5] T. Bogar, M. Sajben, and J. Kroutil, in *AIAA Conference* (AIAA, 1983).

[6] R. Bur, R. Benay, P. Berthouze, and B. Corbel, "Experimental and numerical study of forced shock-wave oscillations in a transonic channel," AIAA Fluid Dyn. Conf. Exhib. **33**, 3470 (2003).

[7] J. C. Robinet and G. Casalis, "Shock oscillations in diffuser modeled by a selective noise amplification," AIAA J. **37**, 453 (1999).

[8] J. Y. Oh, F. Ma, S.-Y. Hsieh, and V. Yang, "Interactions between shock and acoustic waves in a supersonic inlet diffuser," J. Propul. Power **21**, 486 (2005).

[9] R. T. Biedron and T. C. Adamson, Jr., "Unsteady flow in a supercritical supersonic diffuser," AIAA J. **26**, 1336 (1988).

[10] W. H. Moase, M. J. Brear, and C. Manzie, "The forced response of choked nozzles and supersonic diffusers," J. Fluid Mech. **585**, 281 (2007).

[11] P. J. K. Bruce and H. Babinsky, "Unsteady shock wave dynamics," J. Fluid Mech. **603**, 463 (2008).

[12] P. Prasad, *Nonlinear Hyperbolic Waves in Multi-Dimensions* (Chapman & Hall/CRC, 2001).

[13] E. F. Toro, *Reimann Solvers and Numerical Methods for Fluid Dynamics: A Practical Introduction*, 3rd ed. (Springer-Verlag, Berlin Heidelberg, 2009).

[14] M. F. Hamilton and D. T. Blackstock, *Nonlinear Acoustics* (Academic Press, 1998).

[15] J. R. Edwards, "A low-diffusion flux-splitting scheme for Navier-Stokes calculations," Comput. Fluids **26**, 635 (1997).

[16] P. Colella and P. R. Woodward, "The piecewise parabolic method (PPM) for gas-dynamical simulations," J. Comput. Phys. **54**, 174 (1984).

[17] T. W. Roberts, "The behavior of flux difference splitting schemes near slowly moving shock waves," J. Comput. Phys. **90**, 141 (1990).